

A high-contrast imaging polarimeter with a stepped-transmission filter based coronagraph

Cheng-Chao Liu^{1,2,4}, De-Qing Ren^{3,1,2}, Yong-Tian Zhu^{1,2}, Jiang-Pei Dou^{1,2} and Jing Guo^{1,2}

¹ National Astronomical Observatories/Nanjing Institute of Astronomical Optics & Technology, Chinese Academy of Sciences, Nanjing 210042, China; ccliu@niaot.ac.cn

² Key Laboratory of Astronomical Optics & Technology, National Astronomical Observatories/Nanjing Institute of Astronomical Optics & Technology, Chinese Academy of Sciences, Nanjing 210042, China

³ Physics & Astronomy Department, California State University Northridge, 18111 Nordhoff Street, Northridge, California 91330-8268, USA

⁴ University of Chinese Academy of Sciences, Beijing 100049, China

Received 2015 June 29; accepted 2015 November 17

Abstract The light reflected from planets is polarized mainly due to Rayleigh scattering, but starlight is normally unpolarized. Thus it provides an approach to enhance the imaging contrast by inducing the imaging polarimetry technique. In this paper, we propose a high-contrast imaging polarimeter that is optimized for the direct imaging of exoplanets, combined with our recently developed stepped-transmission filter based coronagraph. Here we present the design and calibration method of the polarimetry system and the associated test of its high-contrast performance. In this polarimetry system, two liquid crystal variable retarders (LCVRs) act as a polarization modulator, which can extract the polarized signal. We show that our polarimeter can achieve a measurement accuracy of about 0.2% at a visible wavelength (632.8 nm) with linearly polarized light. Finally, the whole system demonstrates that a contrast of 10^{-9} at $5\lambda/D$ is achievable, which can be used for direct imaging of Jupiter-like planets with a space telescope.

Key words: instrumentation: polarimeter, coronagraph — techniques: polarimetric — methods: laboratory

1 INTRODUCTION

The search for exoplanets is a hot topic and up to now more than 1924 exoplanets have been discovered by using different methods. However, most of them have been detected by indirect methods, such as radial velocity or transit approaches. Although there is preliminary information on the statistics describing the distributions of masses and semi-major axes for these exoplanets, the current catalogs suffer from incompleteness for masses below $0.3 M_J$ (the unit of mass is equal to the total mass of the planet Jupiter) and periods longer than 5.5 yr (<http://exoplanet.eu>). Therefore, direct imaging research will become more important and can be used to characterize the physical parameters of planets, which will challenge the current theory of formation and evolution of planets. However, the direct imaging of exoplanets is extremely challenging due to the close angular separation and extremely high contrast ratio between a planet and its primary star. For example, a contrast of 10^{-10} is required to image Earth-like planets in visible wavelengths at a few λ/D from the parent star, where λ is the working wavelength and D is the aperture size of the primary mirror of the telescope.

A high-contrast coronagraph can be used to tackle diffracted starlight arising from optics that are part of the telescope (Guyon et al. 2006). A complicated wavefront control system can be used to suppress speckle noises to generate a dark hole (DH) due to wavefront distortions from imperfections in the optics (Bordé & Traub 2006). Researchers at the Jet Propulsion Laboratory (JPL) and Princeton University have optimized a small local DH ($X = 3\lambda/D$, $Y = 6\lambda/D$) using two deformable mirrors (DMs) with a large number of actuators, where the contrast can reach the level of 10^{-10} (Trauger & Traub 2007; Kay et al. 2009). However, the DH created by the current technique is too small to apply to a space telescope to directly image Earth-like planets.

In a recent study, it was shown that light directly detected from a star is normally unpolarized, but light reflected from a planet's atmosphere or circumstellar disk is strongly polarized. In Stam's work, a numerical simulation showed that the degree of polarization can reach about 60% for Jupiter-like exoplanets for phase angles near 90° (Stam et al. 2004). Thus, it provides an approach to remove speckle noises and enhance imaging contrast by inducing the imaging polarimetry technique. Also, the polarime-

try can be used to characterize a planet, since the Stokes parameters of the reflected starlight depend strongly on the composition and structure of the planet’s atmosphere (Graham et al. 2007).

Currently, many polarimeters have been developed and used as one of the main components in ground-based planet imaging systems, such as the Gemini Planet Imager (GPI) on the Gemini Telescope, which saw its first light in 2013, and the Zurich Imaging Polarimeter (ZIMPOL) built for SPHERE on VLT UT3, which achieved its first light in 2014 (Perrin et al. 2015; Roelfsema et al. 2010).

In this paper, we propose our unique high-contrast imaging polarimeter coupled with a stepped-transmission based coronagraph. We describe the instrument design, principle and data acquisition in Section 2. The Mueller matrix associated with the instrument and approach used for calibration are shown in Section 3, and Section 4 describes the performance of the polarimeter. We conclude with our results and outline our future work in Section 5.

2 INSTRUMENT DESIGN

Figure 1 presents a schematic diagram showing the optical layout of our polarimetry system. This system is composed of two main components. One is the apodized pupil and the other is the polarimeter. The circular stepped-transmission filter is placed in the optics ahead of the pupil to suppress the diffracted light, which can achieve a contrast of the order 10^{-7} (Ren et al. 2010). Then a polarimeter is inserted after the pupil apodization system, which includes a calibration unit (a polarizer and a zero-order quarter waveplate) and two liquid crystal variable retarders (LCVRs). The LCVRs will be used as a polarization modulator. More details will be presented in Section 2.2.

2.1 Polarimeter Coronagraph

Here we will mainly focus on the design and testing of the polarimetry system, since we use the previously described stepped-transmission based coronagraph. Thus we will present a brief review of the coronagraph and will not discuss it in detail. The amplitude of the electric field is variable in different steps of a stepped-transmission filter. However, it is constant within each step. The metallic material Inconel is deposited on a BK7 substrate and the transmission is controlled by adjusting the thickness of the Inconel. The metallic coating filter consists of 50 steps along the aperture radius. The basic concept of using a stepped-transmission filter for pupil apodization was first proposed by Ren and Zhu (Ren & Zhu 2007). This approach can efficiently suppress the diffracted light from the central star. The stepped-transmission filter coronagraph we use in this polarimeter can achieve a high contrast of $\sim 10^{-7}$ at $5\lambda/D$, which was fully demonstrated in 2010 (Ren et al. 2010).

2.2 Modulation Segment and the Stokes Parameters Acquisition

Two nematic LCVRs manufactured by Thorlabs, which are optimized for 350 to 700 nm, are used to modulate the incoming beam. We use LCVRs instead of waveplates, because this can reduce the effects of mechanical motion. Figure 2 shows the optical configuration of the polarization modulation package.

To obtain the Stokes vector, the polarimeter should take four images in four different modulation states. We adopt the IMAx method to find the Stokes polarization components (Martinez Pillet et al. 2004), in which the retardance of LCVR1 and LCVR2 corresponds to $(315^\circ \ 315^\circ \ 225^\circ \ 225^\circ)$ and $(305.246^\circ \ 54.736^\circ \ 125.246^\circ \ 234.736^\circ)$ respectively. The Stokes I, Q, U, V parameters can be derived from the following formula

$$\begin{pmatrix} I_1 \\ I_2 \\ I_3 \\ I_4 \end{pmatrix} = \begin{pmatrix} 1 & 1/\sqrt{3} & 1/\sqrt{3} & 1/\sqrt{3} \\ 1 & 1/\sqrt{3} & -1/\sqrt{3} & -1/\sqrt{3} \\ 1 & -1/\sqrt{3} & -1/\sqrt{3} & 1/\sqrt{3} \\ 1 & -1/\sqrt{3} & 1/\sqrt{3} & -1/\sqrt{3} \end{pmatrix} \cdot \begin{pmatrix} I \\ Q \\ U \\ V \end{pmatrix}. \quad (1)$$

The LCVR’s phase retardance is generated by applying an associated voltage. However, the phase retardance and voltage relationship may be variable from LCVR1 to LCVR2, which is also a function of the wavelengths. We measured the actual phase retardance and voltage relationship at the test wavelength of 632.8 nm in our laboratory. Figure 2.2 shows the calibration curves of two LCVRs measured in our lab, compared with those provided by the vendor Thorlabs at the same temperature ($T = 23.4$ Celsius) (Wu et al. 1984; Shekwoga Baba & Boudreaux 2007). According to these curves, we should use linear interpolation to work out the required voltages for different kinds of phase retardance.

3 THE METHOD FOR DETERMINING THE INSTRUMENTAL MUELLER MATRIX AND CALIBRATION

The optical elements of the whole instrument will induce additional polarization (up to 5% at visible wavelengths) and influence the measurement accuracy (de Juan Ovelar et al. 2014; Perrin et al. 2010). Therefore, we should calibrate the instrument to derive the Mueller matrix of the instrument, which represents the effects the polarimeter have on the incident polarized starlight. In this part, we use a calibration unit, which is shown in Figure 1, consisting of a linear polarizer and a Thorlabs zero-order quarter waveplate optimized for 632.8 nm. The calibration unit can generate a series of different known polarization states.

3.1 Instrumental Calibration

The input Stokes vector (I, Q, U, V) , S , of the light and the measured Stokes vector, S' , satisfy the following equation

$$S' = M_n \cdot \dots \cdot M_2 \cdot M_1 = M_i \cdot S. \quad (2)$$

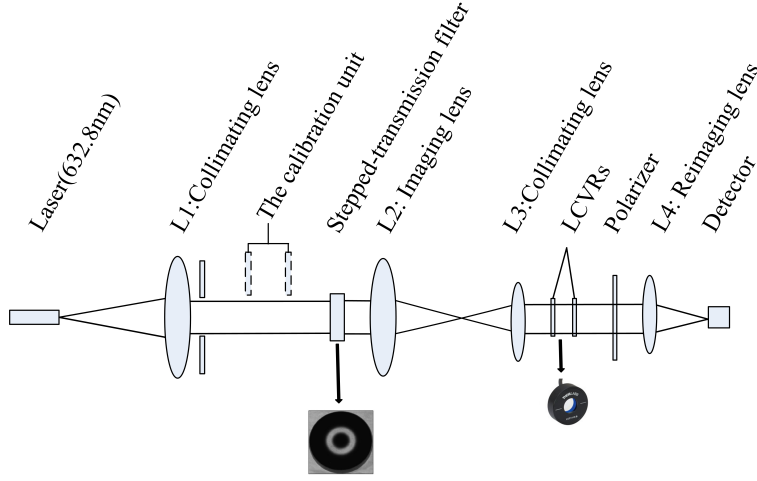


Fig. 1 Optical concept of the polarimeter with the stepped-transmission filter coronagraph, which suppresses light from the central star.

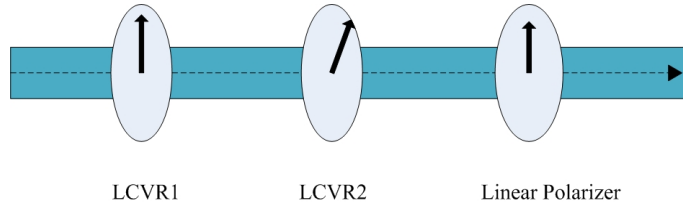


Fig. 2 The configuration of the modulation package. The two LCVRs are mounted with their fast axis at 0° and 45° respectively.

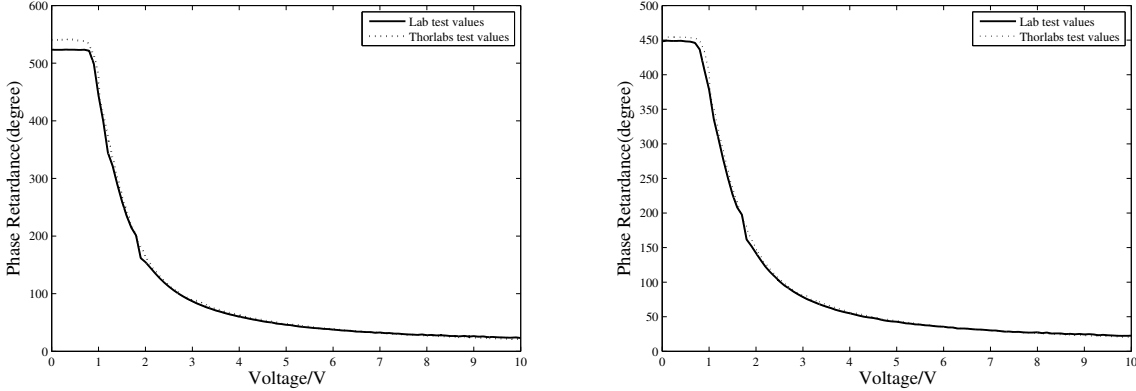


Fig. 3 The calibration curves of two LCVRs. Left: LCVR1. Right: LCVR2.

Here, $M_1 \dots M_n$ represent the Mueller matrices of n optical elements. M_i is a 4×4 Mueller matrix of the instrument, which we need to determine. When the calibration unit is inserted in the optical system, the measured output, S' , can be expressed by

$$S' = M_i \cdot M_r(\theta_i) \cdot M_p(\theta_p) \cdot S. \quad (3)$$

where $M_r(\theta_i)$ and $M_p(\theta_p)$ denote the Mueller matrix of the waveplate retarder and the linear polarizer, respectively. S , $(I_0 \ 0 \ 0 \ 0)^T$, is the input Stokes state. The linear polarizer is fixed ($\theta_p = 0$) and the quarter waveplate retarder (θ_i) is rotated from 0° to 180° in steps of 10° representing one Stokes parameter at a time. Therefore, the

input Stokes states can be described as

$$\begin{aligned} S_{in} &= M_r(\theta_i) \cdot M_p(\theta_p) \cdot S \\ &= I_0/2 \cdot (1, \cos^2 2\theta_i, \sin 2\theta_i \cos 2\theta_i, \sin 2\theta_i)^T. \end{aligned} \quad (4)$$

So far, we know the input states S (4×19) and we can also measure the output states S' (4×19). The instrumental Mueller matrix can be solved by a singular value decomposition.

Figure 4 shows the differences among the measured vector, theoretical input and the value computed by the instrumental Mueller matrix. We note that the fitted value of the input Stokes vector is in good agreement with the ideal input vector.

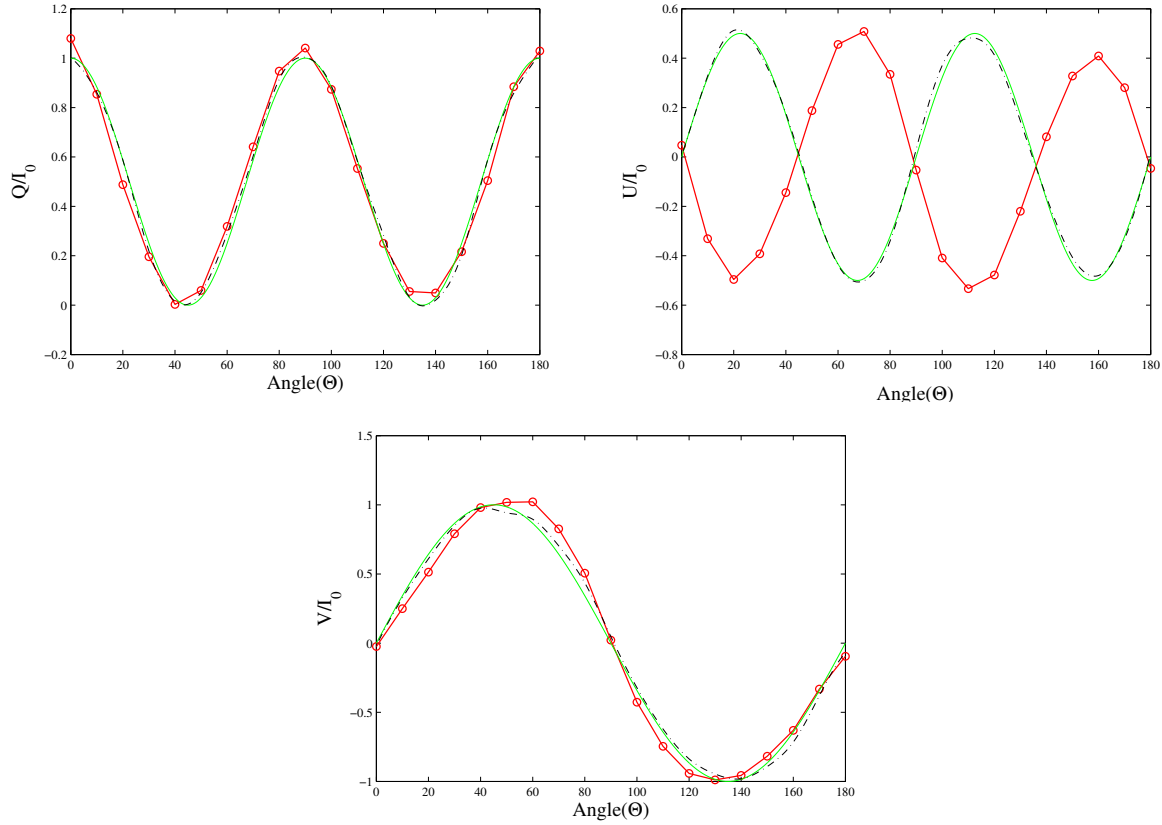


Fig. 4 Stokes vector calibration result. Measured data (solid line with circles), theoretical input (solid line) and the best fit values (dot-dashed line).

From Equation (3) and Figure 4 we can find that the instrumental Mueller matrix is

$$M_i = \begin{pmatrix} +1 & -0.0089 & -0.0237 & +0.0174 \\ -0 & +1.0214 & -0.0020 & -0.0367 \\ -0 & -0.0589 & -0.9860 & -0.2177 \\ +0 & +0.0068 & +0.0552 & +1.0270 \end{pmatrix}. \quad (5)$$

After computing by the above Mueller matrix, for an input beam that is linearly polarized, the accuracy of the polarization measurement can reach the level of about 0.2%. From Figure 4 we find that the improvement in the accuracy after such calibration is significant.

4 THE PERFORMANCE OF THIS POLARIMETER USED IN EXOPLANET DETECTION

This section describes the overall system test and its performance. Two lasers simulate the star and the planet, respectively. The light from the planet laser is polarized by a linear polarizer. Our goal is to detect the faint polarized signal of the planet from the unpolarized starlight and to quantify the level of contrast the polarimeter can achieve.

4.1 Intensity Calibration

The method to calibrate the intensity has been proposed by us in our previous paper (Liu et al. 2015). As is well known, the detection range of a 16-bit CCD camera is only from 0 to 65536. The contrast (10^{-9}) we measure is definitely out of this range. Therefore, we insert neutral density (ND) filters to attenuate the starlight. In our test, the overall level of attenuation is 10^{-8} . Firstly, part of the polarimeter, the stepped-transmission filter and all the linear polarizers should be removed before calibration. Then, we move the positions of the star and planet to the same pixels. Finally, we adjust the exposure time to make the intensity of the star (attenuated by the NDs) and the planet equal to each other. From Figure 5 we can deduce the contrast of the two beams: $0.1/10^8 = 10^{-9}$ (Ren et al. 2010). Once this intensity calibration is done, we will use the polarimeter to detect dim light from the planet.

4.2 Detection of the Faint Polarized Light Reflected by the Planet

According to Section 2.2, we need to take four images under four different modulation states to obtain the Stokes vector. Figure 6 shows the original point spread function (PSF) without the transmission filter (left), the PSF suppressed by the filter (middle) and linearly polarized inten-



Fig. 5 Left panel shows the starlight intensity with an exposure of 0.1 s. Right panel shows the planet light intensity with an exposure of 1 s.

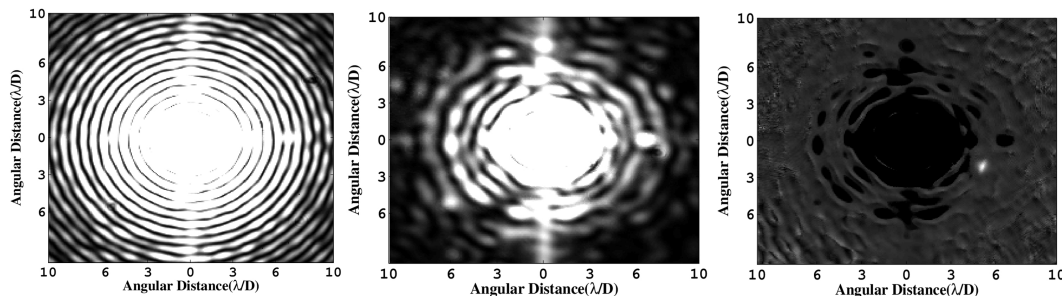


Fig. 6 *Left*: Total intensity of the PSF (without transmission filter). *Middle*: The PSF suppressed by the transmission filter. *Right*: The linearly polarized intensity of the PSF. The whole angular distance from the central star to the edge is $10\lambda/D$.

sity (right) after data reduction. We can see that the dim planet cannot be detected in the presence of the bright star (left and middle). The planet (red circle, left panel) emerges at $5\lambda/D$, while the unpolarized starlight is suppressed by the polarimetry.

This test demonstrates that our polarimeter has the ability to directly detect exoplanets or debris disks and it can also improve the contrast by a factor of at least 100, because the coronagraph can give a contrast of $\approx 10^{-7}$. Due to the instrumental polarization and noise, there is some residual polarized intensity (right). The noise (such as detector read noise) becomes relatively larger with increasing separation from the central star.

5 CONCLUSIONS

The polarimetry technique will become a powerful approach to characterize faint exoplanets and circumstellar disks in the visible wavelengths, where the reflected light is dominant, rather than self luminous light in the infrared. In this work, we have presented the design and performance of our high-contrast polarimeter integrated with a coronagraph for high-contrast imaging. We insert the calibration unit to determine the instrumental Mueller matrix by rotating a quarter waveplate. This improves the measurement accuracy to a level of $\approx 0.2\%$ for the linearly polarized components. The polarimeter can provide an extra contrast of ≈ 100 times at an inner working angular distance of $5\lambda/D$, and the combination of a polarimeter and coronagraph can reach a contrast of 10^{-9} at 632.8 nm. Also, the high-contrast region from $5\lambda/D$ to $10\lambda/D$ on the entire imaging focal plane is larger, which is of great importance

for applying to a space telescope. In addition, the high-contrast region from $5\lambda/D$ to $10\lambda/D$ on the entire imaging focal plane is larger than the DHs created by other groups such as at JPL and Princeton University, which is also of great importance for applying to a space telescope.

This paper demonstrates that the combination of a polarimeter and a coronagraph is a promising technique for imaging of cold planets including Jupiter-like or Earth-like planets with future giant segmented mirror telescopes such as the Thirty Meter Telescope (TMT) or European Extremely Large Telescope (E-ELT) as well as space based telescopes. Since the telescope’s optics will partially affect the polarization, more factors should be considered in practical observations. Meanwhile, a system that can provide a constant temperature is necessary, because the LCVR is affected by variations in temperature. Our ultimate goal is to improve the contrast to the order of 10^{-10} or better on the entire imaging focal plane by solving these problems. Further progress will be discussed in future papers.

Acknowledgements This work was supported by the NSFC (Grant Nos. 11220101001, 11433007, 11328302, 11373005 and 11303064), the “Strategic Priority Research Program” of the Chinese Academy of Sciences (Grant Nos. XDA04070600 and XDA04075200), the special funding for Young Researchers of Nanjing Institute of Astronomical Optics & Technology, and the special fund for astronomy (Grant No. KT2013-022) of CAS. Part of the work described in this paper was carried out at California State University Northridge, with support from the Mt. Cuba Astronomical Foundation.

References

- Bordé, P. J., & Traub, W. A. 2006, *ApJ*, 638, 488
- de Juan Ovelar, M., Snik, F., Keller, C. U., & Venema, L. 2014, *A&A*, 562, A8
- Graham, J. R., Kalas, P. G., & Matthews, B. C. 2007, *ApJ*, 654, 595
- Guyon, O., Pluzhnik, E. A., Kuchner, M. J., Collins, B., & Ridgway, S. T. 2006, *ApJS*, 167, 81
- Kay, J. D., Pueyo, L. A., & Kasdin, N. J. 2009, in Society of Photo-Optical Instrumentation Engineers (SPIE) Conference Series
- Liu, C.-C., Ren, D.-Q., Dou, J.-P., et al. 2015, *RAA (Research in Astronomy and Astrophysics)*, 15, 453
- Martinez Pillet, V., Bonet, J. A., Collados, M. V., et al. 2004, in Society of Photo-Optical Instrumentation Engineers (SPIE) Conference Series, 5487, *Optical, Infrared and Millimeter Space Telescopes*, ed. J. C. Mather, 1152
- Perrin, M. D., Graham, J. R., Larkin, J. E., et al. 2010, in Society of Photo-Optical Instrumentation Engineers (SPIE) Conference Series, 7736, 5
- Perrin, M. D., Duchene, G., Millar-Blanchaer, M., et al. 2015, *ApJ*, 799, 182
- Ren, D., Dou, J., & Zhu, Y. 2010, *PASP*, 122, 590
- Ren, D., & Zhu, Y. 2007, *PASP*, 119, 1063
- Roelfsema, R., Schmid, H. M., Pragt, J., et al. 2010, in Society of Photo-Optical Instrumentation Engineers (SPIE) Conference Series, 7735, 4
- Shekwaga Baba, J., & Boudreaux, P. R. 2007, *Appl. Opt.*, 46, 5539
- Stam, D. M., Hovenier, J. W., & Waters, L. B. F. M. 2004, *A&A*, 428, 663
- Trauger, J. T., & Traub, W. A. 2007, *Nature*, 446, 771
- Wu, S.-T., Efron, U., & Hess, L. D. 1984, *Appl. Opt.*, 23, 3911